Pramāṇa – J. Phys., Vol. 27, No. 6, December 1986, pp. 747–760. © Printed in India.

# Elastic and inelastic scattering of 270 MeV $^3$He particles from $^{58}$Ni, $^{90}$Zr, $^{116}$Sn and $^{208}$Pb

P P SINGH, Q LI*, P SCHWANDT, W W JACOBS, M SABER**, E J STEPHENSON, A SAXENA*** and S KAILAS***†

Indiana University Cyclotron Facility, Indiana 47405, USA
*Academic Sinica, Beijing, China
**Northwestern University, Illinois, USA
***Nuclear Physics Division, Bhabha Atomic Research Centre, Bombay 400 085, India

MS received 15 March 1986; revised 18 June 1986

**Abstract.** Differential cross-section angular distributions for the elastic scattering of 270 MeV $^3$He particles from $^{58}$Ni, $^{90}$Zr, $^{116}$Sn and $^{208}$Pb have been measured. Optical model analysis of the cross-sections has yielded the optical model parameters for $^3$He particles at 270 MeV. Angular distributions have also been measured for the inelastic excitation of the low-lying levels in the above mentioned nuclei. A collective model analysis using the distorted wave Born approximation (DWBA) of these cross-sections with the distorted waves generated by the optical model parameters determined from the elastic scattering analysis, has yielded the reduced transition probability (B(EL)) values consistent with those reported in the literature.

**Keywords.** Elastic scattering; inelastic scattering; helium-3 particles at 270 MeV; nickel-58; zirconium-90; tin-116; lead-208 targets; optical model; distorted wave Born-approximation analysis.

**PACS No. 25-60**

## 1. Introduction

As a part of the programme to study the excitation of the giant resonance region in $^{58}$Ni, $^{90}$Zr, $^{116}$Sn and $^{208}$Pb utilising the 270 MeV $^3$He particles, we have measured the elastic and the inelastic scattering of $^3$He particles at this energy. The inelastic scattering measurements are mainly for the low-lying states of the various target nuclei. For $^3$He particle energies greater than 100 MeV, the elastic scattering measurements have been reported at 217 MeV (Willis *et al* 1973), 130 MeV (Djaloeis *et al* 1978) and in the energy region 90–120 MeV (Hyakutake *et al* 1978, 1980). The present work at 270 MeV is perhaps the highest energy at which the elastic and the inelastic scattering data from $^3$He particles are being reported. Langevin-Joliot *et al* (1982) reported ($^3$He, $^4$He) reaction at 280 MeV $^3$He energy, but the analysis of the $^3$He elastic or inelastic cross-sections has not been published.

The experimental details of the measurements are given in § 2. The analysis and the results for the elastic and inelastic scattering data are given in § 3. The conclusions are given in § 4.

†To whom all correspondence should be addressed.

## 2. Experimental procedure

The present measurements have been carried out utilising the 270 MeV $^3$He particle beams available from the Indiana University Cyclotron Facility (IUCF). The isotopically enriched targets of $^{58}$Ni (99 %), $^{90}$Zr (98 %), $^{116}$Sn (96 %) and $^{208}$Pb (99 %) ranging in thickness from 10 to 100 mg/cm$^2$ were used. The scattered particles were detected using the QDDM spectrometer (Bent *et al* 1981). The differential cross-section measurements were carried out in the angular range of $\theta \sim 6°$ to 32° in steps of 0·75° or 1·5°. The angular resolution was kept at 0·2° for $\theta < 27°$ and 0·4° for $\theta > 27°$. Beam current on the target ranged from 1·0 to 50 (particle) nA.

The measured differential cross-sections for the elastic scattering for all target nuclei are plotted in figure 1. The inelastic scattering to various low-lying states of $^{58}$Ni, $^{90}$Zr, $^{116}$Sn and $^{208}$Pb are presented in figures 3–6 respectively. The elastic scattering cross-sections have absolute errors of the order of $\pm$ 5 % arising mainly due to target non-uniformity and uncertainties in target thicknesses. The inelastic scattering data have uncertainties between 5 and 10 %, composed of errors due to counting statistics, target thickness and target non-uniformity and the peak fitting procedure followed in the data analysis of overlapping levels.

## 3. Analysis and results

### 3.1 *Elastic scattering*

As can be seen from figure 1, the angular distribution data exhibit a few strong oscillations characteristic of Fraunhoffer diffraction followed by a rather smooth exponential fall-off. Conventional optical model analysis of the elastic cross-sections, using the code SNOOPY (Schwandt 1981), has yielded the parameters as listed in table 1. The optical potential employed is parametrized as,

$$U(r) = U_{\text{Coul}}(r) - V_R f_I(r) - iV_I f_I(r). \tag{1}$$

Here $U_{\text{Coul}}$ represents the Coulomb potential and $V_R$ and $V_I$ are the strengths of the real and the imaginary parts of the complex nuclear potentials respectively. The form factor $f_R(r)$ ($f_R(r)$) of the real (imaginary) part of the potential was assumed to have a Woods-Saxon form, characterized by a half-value radius $r_R A_T^{1/3}$ ($r_I A_T^{1/3}$) and diffuseness, $a_R(a_I)$. ($A_T$ = target mass number).

The code SNOOPY uses relativistic kinematics in the optical model calculation. Starting from the set of parameters found best suitable at $E = 217$ MeV (Willis *et al* 1973) we optimized the parameters (table 1) to get the best fit to the data. The best fit theoretical curves along with the experimental data are shown in figure 1. The optical model fit to the experimental cross-sections is, in general, quite good for all the targets. The structures and the absolute cross-sections are better reproduced, within experimental uncertainties, for the angles forward of 25° than for the ones larger than 25. The optical model predictions do show discrepancies as compared to experimental data, in some angular regions, (particularly some of the minima in $\sigma/\sigma_R$ plots) and they vary with the target. A better fit could be obtained by varying all the parameters, but due to limited angular range of the experimental cross-sections, such an exercise was not considered useful.

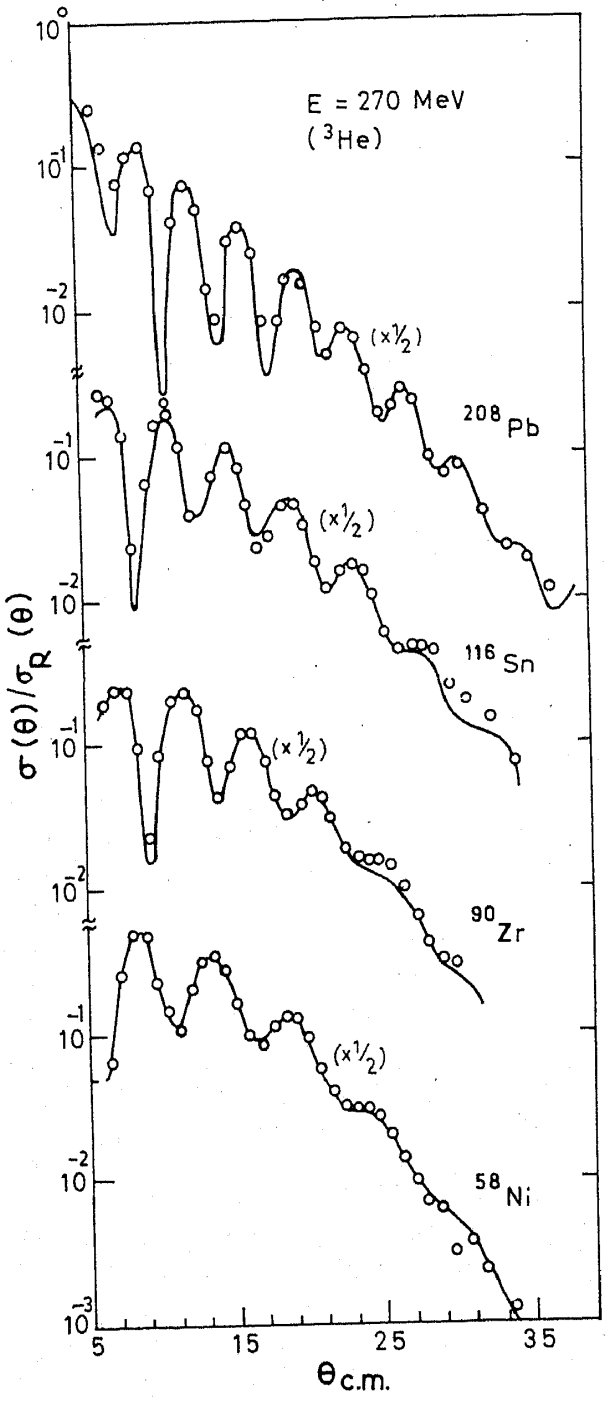


**Figure 1.** Differential cross-section angular distributions for the elastic scattering of $^{3}$He particles by $^{58}$Ni, $^{90}$Zr, $^{116}$Sn and $^{208}$Pb. The curves are the optical model fits to the data. $\theta$'s are in degrees.

The volume integral per projectile-target pair is defined as

$$J_R = \int |V_R| f_R(r)\, \mathrm{d}\tau/(A_P A_T),$$
$$J_I = \int |V_I| f_I(r)\, \mathrm{d}\tau/(A_P A_T), \qquad (2)$$

**Table 1.** Optical model parameters $^{58}$Ni, $^{90}$Zr, $^{116}$Sn, $^{208}$Pb + $^{3}$He (270 MeV).

| | $^{58}$Ni | $^{90}$Zr | $^{116}$Sn | $^{208}$Pb |
|---|---|---|---|---|
| $V_R$ (MeV) | 67 | 69 | 66 | 71 |
| $r_R$ (fm) | 1·24 | 1·24 | 1·27 | 1·25 |
| $a_R$ (fm) | 0·85 | 0·83 | 0·86 | 0·86 |
| $V_I$ (MeV) | 21 | 23 | 23 | 18 |
| $r_I$ (fm) | 1·41 | 1·39 | 1·40 | 1·43 |
| $a_I$ (fm) | 0·79 | 0·79 | 0·66 | 0·81 |
| $r_c$ (fm) | 1·35 | 1·35 | 1·35 | 1·35 |
| $J_R$ (MeV fm$^3$) | 233 | 224 | 224 | 219 |
| $J_I$ (MeV fm$^3$) | 99 | 100 | 96 | 80 |
| $\sigma_R$ (mb) | 1365 | 1745 | 1885 | 2775 |

Note. Half value radius = $r_x A_T^{1/3}$ fm ($x = R$ or $I$); Coulomb radius = $r_c A_T^{1/3}$ fm; $\sigma_R$ = Reaction cross-section.

respectively for the real and the imaginary parts of the optical potential. In the above equation $A_P$ and $A_T$ represent the mass number of the projectile and the target nuclei, respectively. The volume integrals $J_R$ and $J_I$ are found to be less ambiguous quantities to study the energy and/or target mass dependences of the optical potential. We have plotted in figure 2, the values of $J_R$ and $J_I$ in the 100–270 MeV region using the results of the optical model analysis of 100–217 MeV $^{3}$He elastic scattering (Willis *et al* 1973; Djaloeis *et al* 1978; Hyakutake *et al* 1978, 1980), along with those of this report. It is clear from an inspection of figure 2 (top part) that $J_R$ decreases linearly with the bombarding energy of $^{3}$He. The decrease of $J_R$ with energy can be anticipated due to the non-locality effect (Hodgson 1966) and the intrinsic energy dependence arising from the energy dependence of the separation distance of the two-body effective interactions (Sinha *et al* 1973).

The volume integrals $J_I$ plotted in the lower part of figure 2. The energy dependence seen in the case of $J_I$ is not as significant as that observed for $J_R$.

We have fitted the $J_R$ and $J_I$ values in the energy region 100 to 270 MeV, and for $A = 40$–$208$ using the following functional form for the volume integrals $J$ that was found (Gupta and Murthy 1982; Gupta *et al* 1985) successful in explaining the data for energies below 50 MeV/nucleon. With the functional form

$$J_x = \left[ J_{0x}(1-\alpha_x E^*) + \left(\frac{N_T - Z_T}{A_T}\right) J_{1x}(1-\beta_x E^*) \right] (1 + r_x A_T^{-1/3})$$

with $$E^* = E - 2(1{\cdot}44\, Z_T / A_T^{1/3}), \tag{3}$$

the effective projectile energy and $X = R$ (real) or $I$ (imaginary) part, the volume integral data have been fitted, varying the parameters $J_{0x}$, $J_{1x}$, $\alpha_x$, $\beta_x$ and $r_x$. We assumed an error of $\pm$ 5% on the $J$ values in carrying out the fit. As the five parameters mentioned above are correlated one should be cautious in identifying the terms $J_{0x}$ and $J_{1x}$ with the isoscalar and the isovector parts of the interaction. The values of the various parameters found from the above procedure in the energy region 100–270 MeV are listed in table 2. The solid lines in upper part of figure 2 represent the predictions for

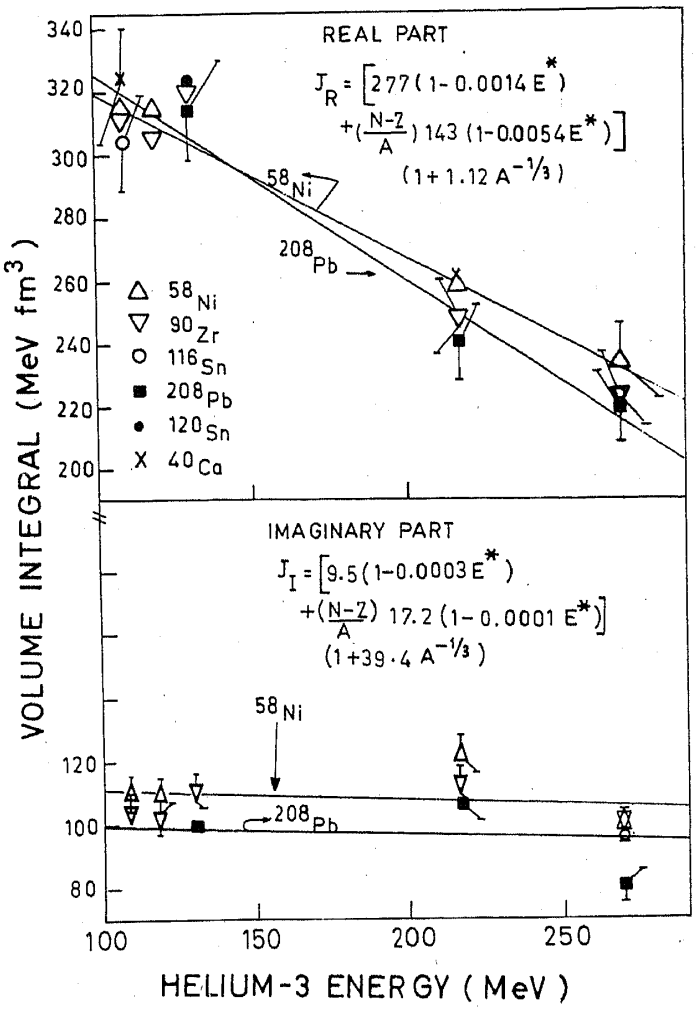


**Figure 2.** Volume integrals per target-projectile pair, $J_R$ for the real part and $J_I$ for the imaginary part are plotted as a function of $^3$He energy. The continuous and the dashed lines represent the calculations using (3) for $^{58}$Ni and $^{208}$Pb.

**Table 2.** Parameters to fit the volume integrals $J_R$, $J_I$.

| | | | |
|---|---|---|---|
| $J_{0R}$ | 277 | $J_{0I}$ | 9·5 |
| $\alpha_R$ | $1{\cdot}40 \times 10^{-3}$ | $\alpha_I$ | $2{\cdot}54 \times 10^{-4}$ |
| $J_{1R}$ | 143 | $J_{1I}$ | 17·2 |
| $\beta_R$ | $5{\cdot}43 \times 10^{-3}$ | $\beta_I$ | $1{\cdot}41 \times 10^{-4}$ |
| $r_R$ | 1·12 | $r_I$ | 39·4 |

Note: $J$'s in MeV fm$^3$; $\alpha$'s, $\beta$'s in fm$^3$.

$^{208}$Pb and $^{58}$Ni, using expression (3). It appears that $A_T$ dependence of $J_R$ is not very significant for lower $E$ values and within the errors on $J_R$ the values of $^{58}$Ni are not different from those obtained for $^{208}$Pb. However, for larger $E$ values beyond 200 MeV there are noticeable differences between the $J_R$ values of $^{58}$Ni and $^{208}$Pb.

The solid lines on the lower part of figure 2 represent the predictions (using (3)) for $^{58}$Ni and $^{208}$Pb. The two lines roughly enclose the observed values of $J_I$ for the various target masses. It is found that the $J_R$ and $J_I$ values determined at 270 MeV for $^{208}$Pb in the present work are 219 MeV fm$^3$ and 80 MeV fm$^3$, respectively. These are quite different from the values of 166 MeV fm$^3$ and 99 MeV fm$^3$, respectively obtained from extrapolations of the formulae found successful in explaining the data for energies upto 50 MeV/nucleon (Gupta and Murthy 1982; Gupta *et al* 1985).

### 3.2 *Inelastic scattering*

The angular distribution data for the strongly excited low-lying levels, in the various nuclei are plotted in figures 3, 4, 5 and 6 for the target nuclei $^{58}$Ni, $^{90}$Zr, $^{116}$Sn and $^{208}$Pb, respectively. The measurements on the low-lying states serve two purposes. First, they give in an independent way, irrespective of any theoretical calculation, the angular distribution shapes for states with $J^\pi = 2^+, 3^-, 4^+$ and $5^-$. These shapes serve

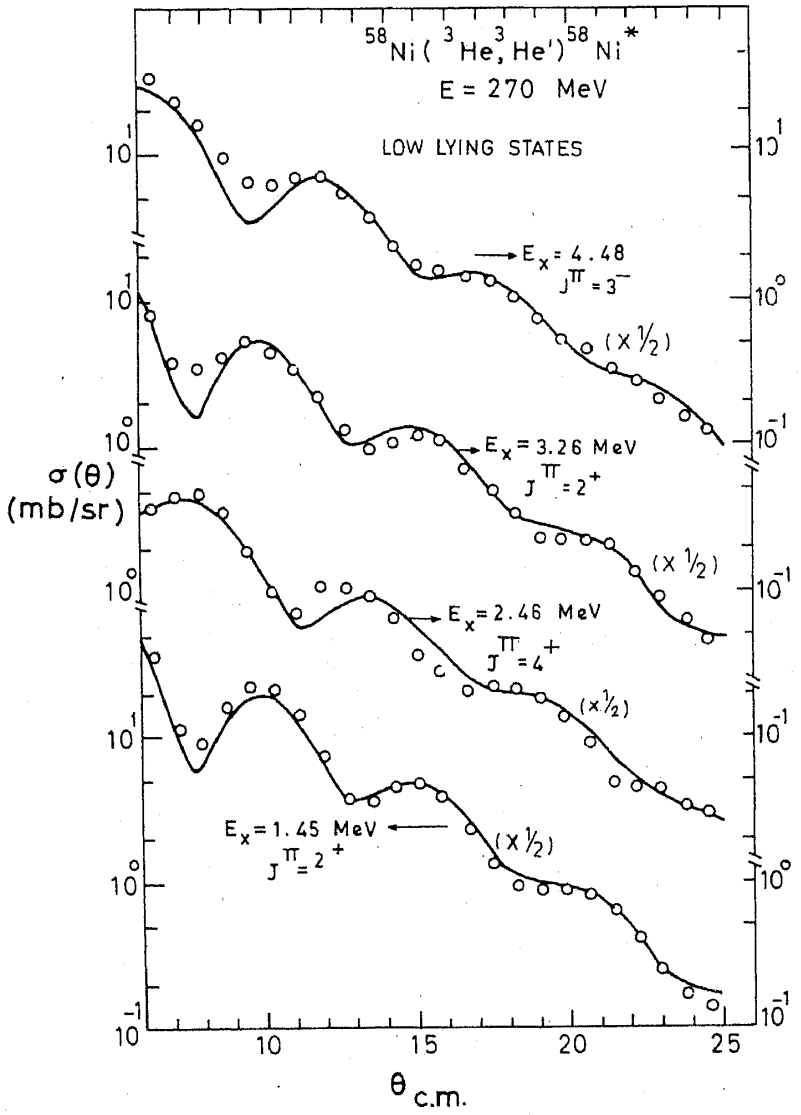


**Figure 3.** Angular distribution data for the low-lying states in $^{58}$Ni. The solid curves are the predictions from the collective model. $\theta$'s are in degrees.

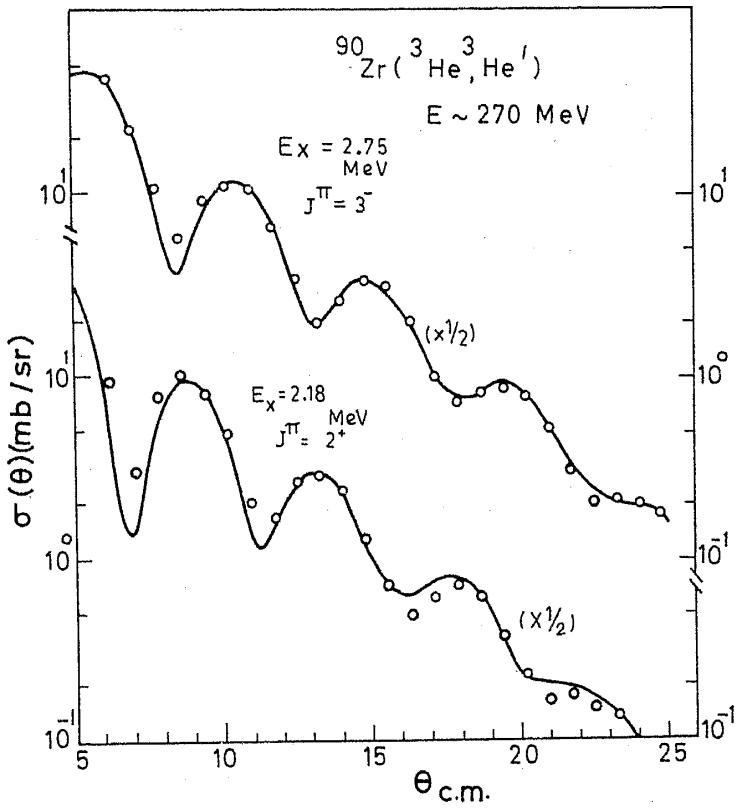


**Figure 4.** Angular distribution data for the low-lying states in $^{90}$Zr. The solid curves are the predictions from the collective model. $\theta$'s are in degrees.

as guides for the behaviour to be expected for multipoles in the giant resonance region. Second, if we can explain satisfactorily with a macroscopic collective model (DWBA) the data for the low-lying states with known $J^\pi$ values, then we can extend these calculations with some confidence in predicting the $\sigma(\theta)$ angular distributions for the various multipolarities observed in the giant resonance region. The inelastic scattering data are compared with the collective model DWBA predictions. In all the calculations a complex transition potential has been used and the effects of Coulomb excitation have been included. The radial part of the interaction potential for exciting a multipole ($L$) vibration is given as

$$V_L = \beta_R r_R A_T^{1/3} \frac{\mathrm{d}V_R(r)}{\mathrm{d}r} + \beta_I r_I A_T^{1/3} \frac{\mathrm{d}V_I(r)}{\mathrm{d}r}, \tag{4}$$

where $V_R(r)$ and $V_I(r)$ are the real and the imaginary parts of the optical potential obtained from fits to the elastic scattering data. $\beta_R$ and $\beta_I$ are the deformation parameters for the real and the imaginary parts respectively. The calculations have been performed using the computer code DWUCK-4 (Kunz 1982) with relativistic kinematics. The calculations have been made assuming $\beta_R = \beta_I$. The values of $\beta$'s were extracted by normalising the observed cross-sections with those of DWBA so that,

$$\beta^2 = \frac{\sigma(\theta)_{\text{expt}}}{\sigma(\theta)_{\text{DWBA}}}. \tag{5}$$

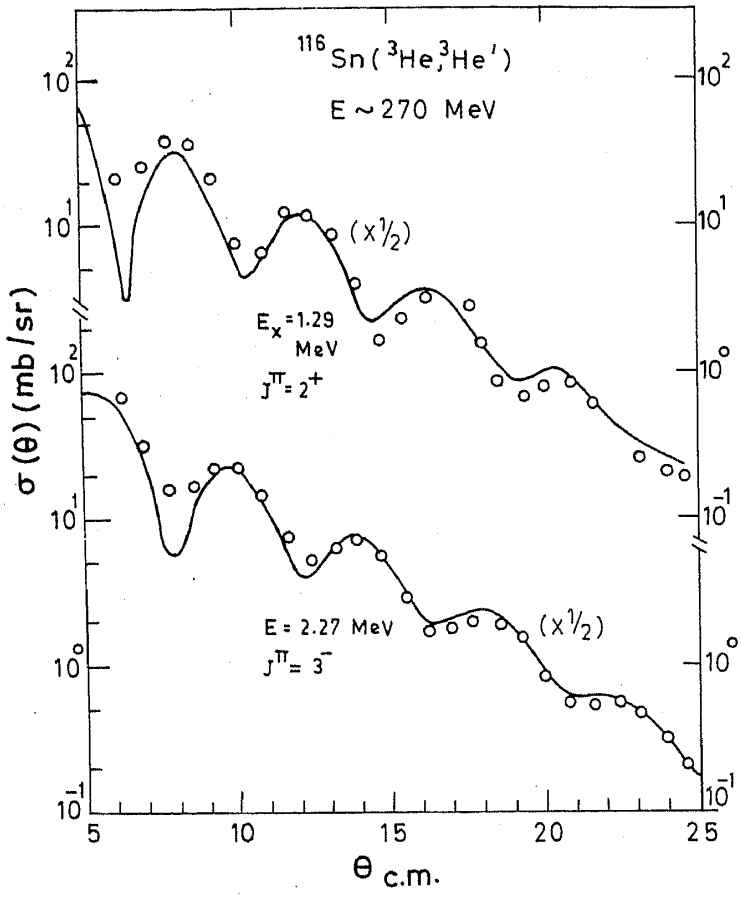


**Figure 5.** Angular distribution data for the low-lying states in $^{116}$Sn. The solid curves are the predictions from the collective model. $\theta$'s are in degrees.

Since in the optical model analysis of the elastic cross-sections (table 1) we have $r_R \neq r_I$, we take the deformation length for the optical model potential, $\delta_{\text{opt}}$, for the various target nuclei as

$$\delta_{\text{opt}} = \beta(r_R A_T^{1/3} + r_I A_T^{1/3})/2 \tag{6}$$

As seen from figures 3 through 6, the macroscopic collective model DWBA calculation gives a reasonable account of the observed inelastic excitation of the low-lying states of various multipolarities. There, however, are some quantitative discrepancies. In the case of Ni (figure 3) for the $4^+$, 2·46 MeV state the calculated positions of the second maxima are at higher angles than observed. For Pb while the data for the strongly excited $3^-$ state is explained well by the DWBA calculation, it is not so for the relatively weakly excited $2^+$ state (figure 6). The largest discrepancies are noticed for the $2^+$ state in Pb. This may be mainly due to the uncertainties involved in the experimental determination of the cross-section for this state. It may be possible to improve the agreement between theory and experiment in certain cases with suitable changes in parameters. But such an attempt was considered not worthwhile as the overall quality of the DWBA predictions has been generally good.

The values of the reduced transition probabilities $B$(EL), were calculated, in both

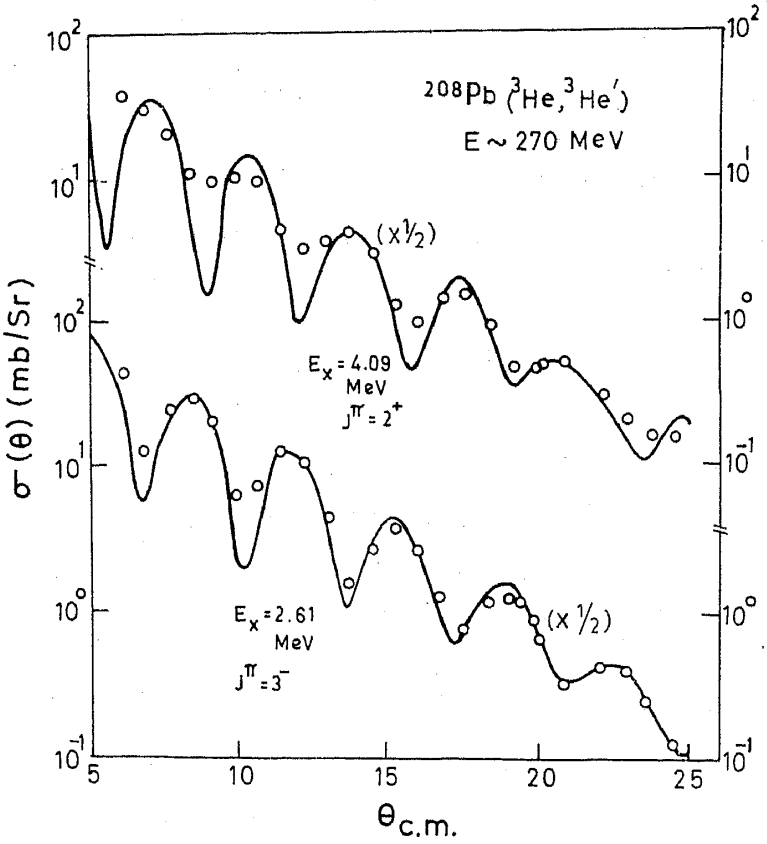


**Figure 6.** Angular distribution data for the low-lying states in $^{208}$Pb. The solid curves are the predictions from the collective model. $\theta$'s are in degrees.

uniform and Fermi density distributions using the following relations:

$$B(\mathrm{EL})_U = \delta^2_{\mathrm{opt}} (Z_T/4\pi)^2 \, 9 \, R_m^{2L-2} \quad \text{(uniform)} \quad \mathrm{e}^2\,\mathrm{fm}^{2L}, \tag{7}$$

$$B(\mathrm{EL})_F = (\delta_{\mathrm{opt}})^2 (Z_T/4\pi)^2 (L+2)^2 \langle r^{L-1} \rangle^2 \quad \text{(Fermi)} \quad \mathrm{e}^2\,\mathrm{fm}^{2L}. \tag{8}$$

$$(R_m = 1{\cdot}2\, A_T^{1/3})$$

For the Fermi distribution, the value of the half density radius was adopted as $R_F = 1{\cdot}115\ A_T^{1/3} - 0{\cdot}53\ A_T^{-1/3}$ and of diffuseness as $a_F = 0{\cdot}568$ fm, following the analysis of Bernstein (1969).

In table 3, we have listed the $B(\mathrm{EL})$ values obtained for the various low-lying levels in $^{58}$Ni, $^{90}$Zr, $^{116}$Sn and $^{208}$Pb. From the $B(\mathrm{EL})_e$ values obtained from electron scattering experiments, the proton deformation lengths $\delta_p$ have been deduced using the expression

$$\delta_p^2 = \frac{B(\mathrm{EL})_e}{e^2} (4\pi/Z_T)^2 \frac{1}{(L+2)^2 \langle r^{L-1} \rangle^2}. \tag{9}$$

In table 4 the $\delta$ values from other determinations are compiled. In table 3 we have listed the average values (from table 4), $\langle \delta \rangle$, $\delta_{\mathrm{opt}}$ (present work for $^3$He), and $\delta_p$ values and made a comparison of them.

In general, within experimental uncertainties, the values of $\delta_{\mathrm{opt}}$ extracted from the

**Table 3.** $\delta_{opt}$, $B(EL)$, $\delta_p$ and $\langle\delta\rangle$ values.

| Nucleus | $E_x$ (MeV) | $J^\pi$ | $\delta_{opt}$ (fm) | $B(EL)e^2$ $U$ | $fm^{2L}$ $F$ | $\delta_p$ (fm) | $\langle\delta\rangle$ (fm) |
|---|---|---|---|---|---|---|---|
| $^{58}$Ni | 1·45 | $2^+$ | 0·773 ± 0·062 | 576 | 652 | 0·711 ± 0·020 | 0·890 ± 0·118 |
| | 2·46 | $4^+$ | 0·312 ± 0·025 | 43688 | 76708 | 0·276 ± 0·008 | 0·364 ± 0·077 |
| | 3·26 | $2^+$ | 0·407 ± 0·033 | 160 | 181 | 0·400 ± 0·010 | 0·360 ± 0·045 |
| | 4·52 | $3^-$ | 0·656 ± 0·039 | 8950 | 11915 | 0·685 ± 0·027 | 0·733 ± 0·047 |
| $^{90}$Zr | 2·18 | $2^+$ | 0·449 ± 0·036 | 531 | 562 | 0·495 ± 0·049 | 0·432 ± 0·054 |
| | 2·75 | $3^-$ | 0·701 ± 0·021 | 37484 | 43690 | 0·980 ± 0·173 | 0·877 ± 0·080 |
| $^{116}$Sn a) | 1·29 | $2^+$ | 0·645 ± 0·065 | 2030 | 2082 | 0·598 ± 0·027 | 0·713 ± 0·079 |
| | 2·27 | $3^-$ | 0·776 ± 0·058 | 100,624 | 110,139 | 0·667 ± 0·033 | 0·806 ± 0·122 |
| $^{208}$Pb | 2·61 | $3^-$ | 0·722 ± 0·048 | 510,499 | 497,446 | 0·807 ± 0·065 | 0·821 ± 0·010 |
| | 4·09 | $2^+$ | 0·532 ± 0·054 | 5482 | 5322 | 0·411 ± 0·033 | 0·399 ± 0·052 |

*Note* a. The error on $\delta_p$ value has been assumed to be ± 5%.

**Table 4.** $\delta$ values from other works.

| Nucleus | $J^\pi$ | $E_x$ (MeV) | $\delta$ (fm) | Method | References |
|---|---|---|---|---|---|
| $^{58}$Ni | $2^+$ | 1·45 | 0·711 | $(e, e')$ | 1 |
| | | | 1·00 | $(\alpha, \alpha')$ | 2 |
| | | | 0·85 | $(n, n')$ | 3 |
| | | | 0·99 | Low $E$ $(p, p')$ | 3 |
| | | | 0·90 | High $E$ $(p, p')$ | 4 |
| | | | $\langle\delta\rangle = 0·890 \pm 0·118$ | | |
| | $4^+$ | 2·46 | 0·276[a] | $(e, e')$ | 5 |
| | | | 0·403 | High $E$ $(p, p')$ | 4 |
| | | | 0·414 | $(\alpha, \alpha')$ | 6 |
| | | | $\langle\delta\rangle = 0·364 \pm 0·077$ | | |
| | $2^+$ | 3·26 | 0·40 | $(e, e')$ | 4 |
| | | | 0·370 | High $E$ $(p, p')$ | 4 |
| | | | 0·311 | $(\alpha, \alpha')$ | 2 |
| | | | $\langle\delta\rangle = 0·360 \pm 0·045$ | | |
| | $3^-$ | 4·52 | 0·685 | $(e, e')$ | 1 |
| | | | 0·779 | High $E$ $(p, p')$ | 4 |
| | | | 0·736 | $(\alpha, \alpha')$ | 2 |
| | | | $\langle\delta\rangle = 0·733 \pm 0·047$ | | |
| $^{90}$Zr | $2^+$ | 2·18 | 0·495 | $(e, e')$ | 4 |
| | | | 0·456 | $(n, n')$ | 3 |
| | | | 0·38 | Low $E$ $(p, p')$ | 3 |
| | | | 0·465 | High $E$ $(p, p')$ | 4 |
| | | | 0·44 | $(\alpha, \alpha')$ | 3 |
| | | | 0·355 | Low $E$ $(p, p')$ | 7 |
| | | | $\langle\delta\rangle = 0·432 \pm 0·054$ | | |

| | | | | | |
|---|---|---|---|---|---|
| | $3^-$ | 2·75 | 0·980 | $(e, e')$ | 4 |
| | | | 0·889 | High $E$ $(p, p')$ | 4 |
| | | | 0·79 | Low $E$ $(p, p')$ | 7 |
| | | | 0·85 | $(\alpha, \alpha')$ | 6 |
| | | | $\langle \delta \rangle = 0{\cdot}877 \pm 0{\cdot}080$ | | |
| $^{116}$Sn | $2^+$ | 1·29 | 0·598 | $(e, e')$ | 8 |
| | | | 0·759 | $(\alpha, \alpha')$ | 9 |
| | | | 0·673 | $(n, n')$ | 3 |
| | | | 0·797 | Low $E$ $(p, p')$ | 10 |
| | | | 0·740 | High $E$ $(p, p')$ | 11 |
| | | | $\langle \delta \rangle = 0{\cdot}713 \pm 0{\cdot}079$ | | |
| | $3^-$ | 2·27 | 0·667 | $(e, e')$ | 8 |
| | | | 0·892 | Low $E$ $(p, p')$ | 10 |
| | | | 0·860 | $(\alpha, \alpha')$ | 9 |
| | | | $\langle \delta \rangle = 0{\cdot}806 \pm 0{\cdot}122$ | | |
| $^{208}$Pb | $3^-$ | 2·61 | 0·807 | $(e, e')$ | 4 |
| | | | 0·83 | Low $E$ $(p, p')$ | 7 |
| | | | 0·825 | High $E$ $(p, p')$ | 4 |
| | | | 0·822 | $(\alpha, \alpha')$ | 12 |
| | | | $\langle \delta \rangle = 0{\cdot}821 \pm 0{\cdot}010$ | | |
| | $2^+$ | 4·09 | 0·411 | $(e, e')$ | 4 |
| | | | 0·37 | Low $E$ $(p, p')$ | 7 |
| | | | 0·466 | High $E$ $(p, p')$ | 4 |
| | | | 0·348 | $(\alpha, \alpha')$ | 12 |
| | | | $\langle \delta \rangle = 0{\cdot}399 \pm 0{\cdot}052$ | | |

[a] The average value of the ratios of $\delta$'s from Afanasev *et al* (1970) to those of Crannell *et al* (1961) for the $2^+, 3^-$ states is 0·71. The value for the $4^+$ state is available only from Crannell *et al* (1961). This value is divided by 1·4 and listed in the table (normalized value).

1. Afanasev *et al* (1970); 2. Jarvis *et al* (1967); 3. Bernstein *et al* (1981b); 4. Gazzaly *et al* (1982); 5. Crannell *et al* (1961); 6. Bernstein (1969); 7. Fujita *et al* (1985); 8. Curtis *et al* (1968); 9. Bingham *et al* (1969); 10. Wiencke *et al* (1983); 11. Liljestrand *et al* (1979); 12. Harakeh *et al* (1979).

present work agree with the corresponding values of $\langle \delta \rangle$ and $\delta_p$ for most transitions in all the four nuclei (see table 3). However a close inspection of the $\delta_{\text{opt}}$ values extracted from the present work and the $\delta_p$ values obtained from electron scattering reveals noticeable differences between them. These differences may be due to the expectation (Bernstein *et al* 1981a) that the deformation of the proton and the neutron density distribution may not be the same. Strictly speaking as pointed out by Bernstein *et al* (1981b) the deformation length in hadron scattering should be written as

$$\delta_{\text{opt}} = \frac{b_p^F Z_T \delta_p + b_n^F N_T \delta_n}{b_p^F Z_T + b_n^F N_T} = \frac{Z_T \delta_p + K N_T \delta_n}{Z_T + K N_T}, \tag{10}$$

where $\delta_p$ and $\delta_n$ are the proton and the neutron deformation lengths respectively and $b_p^F$ and $b_n^F$ are the interaction strength of hadron field with target protons and neutrons respectively. The parameter $K = b_n^F / b_p^F$ depends on the projectile. In effect there is a probe dependence introduced in the determination of the deformation lengths. Thus, if

one knows the value of $K$ and $\delta_p$ then, one can determine the value of $\delta_n$, using the above equation. Knowledge of $\delta_p$ and $\delta_n$ in turn can be used to determine the ratio

$$M_n/M_p = N\delta_n/Z\delta_p \tag{11}$$

of the neutron and the proton transition matrix elements and compared with values of this ratio obtained by using other probes. Such a comparison provides a consistency check on the measured $\delta_{opt}$ values.

$K$ is defined as $(V_{IS}+V_{IV})/(V_{IS}-V_{IV})$ where $V_{IS}$ is the isoscalar and $V_{IV}$ is the isovector interaction of the probe with the target nucleus. In principle one can determine the values of $V_{IS}$ and $V_{IV}$ potentials from an optical model analysis of the $^3$He-nucleus elastic scattering cross-section. In practice due to correlation among various parameters it is not possible to obtain unambiguous values for $V_{IV}$ in particular. Various attempts to determine $V_{IV}$ have yielded values of $V_{IV} \sim 0{\cdot}14\ V_{IS}$ (Hyakutake *et al* 1980) and $V_{IS} \sim V_{IV}$ (Willis *et al* 1973). Our attempts in this respect were not any more successful. One will need complementary elastic cross-section of triton from the same target to be combined with those of $^3$He to determine $V_{IV}$ with better accuracy. In view of this situation we have resorted to the folding model for estimating the values of $V_{IS}$ and $V_{IV}$. We obtain these values for $^3$He energy of $E$ in terms of $V_{IS}$ and $V_{IV}$ of the proton/neutron at the corresponding energy per nucleon of $E/3$. Thus one can define,

$$V_{IS}(^3\text{He}) \approx 3\,V_{IS}(p \text{ or } n),$$

$$V_{IV}(^3\text{He}) \simeq V_{IV}(p).$$

For $E_{p/n} \sim 90$ MeV, $V_{IS} \simeq 36$ MeV and $V_{IV} \simeq 6$ MeV (Bhattacharya and Kailas 1983). With these values one can get a value of $K \simeq 1{\cdot}1$. It has been argued (Gupta and Murthy 1982) that $V_{IV}(^3\text{He}) \sim \frac{1}{3}V_{IV}$ expected from the folding model. This leads to a value of $K \sim 1$, which is not very far from the value given by the folding model. The $\delta_n$ value has been determined using (10) by combining the $\delta_{opt}$ value obtained for $^3$He in the present work with $\delta_p$ value from electron scattering data and taking $K = 1$.

The values of $(M_n/M_p)$ obtained using $\delta_p$ and $\delta_n$ values in (11) are listed in table 5, which also includes the values reported in the literature (Gazzaly *et al* 1982; Bernstein *et al* 1981; Madsen *et al* 1983). The values of $(M_n/M_p)$ for all the states deduced from the present measurements for Ni agree rather well with those reported by Gazzaly *et al* (1982) and those obtained by Bernstein *et al* (1981b). Again for the $2^+$ state in Zr our value is in good agreement with the values of Gazzaly *et al* (1982) and Bernstein *et al* (1981). A major discrepancy between our and Gazzaly values is for $3^-$ state in Zr. For Sn our value is in good accord with that of Bernstein *et al* (1981b). In the case of Pb, for the $2^+$ state all the three works agree. Again there are differences between our and Gazzaly's values for the $3^-$ state in Pb. Overall, it appears that the values of transition matrix elements deduced from the DWBA analysis of $^3$He inelastic cross-sections are in good agreement with those reported in the literature.

The $(M_n/M_p)$ values obtained in the present work can be compared with the predictions of the homogeneous collective model according to which $M_n/M_p = N/Z\cdot(\delta_n = \delta_p)$. It is found (table 5) that the $(M_n/M_p)$ values obtained in some cases (e.g. $2^+$ states in Ni, Zr, Sn), within errors agree with the homogeneous model predictions. However, the $(M_n/M_p)$ values determined in some other cases (e.g. $3^-$ states in Zr, Sn) differ considerably from those expected from the homogeneous model. The present

**Table 5.** $(M_n/M_p)$ values.

| Nucleus | $E_x$ (MeV) | $J^\pi$ | $\delta_{opt}$ (fm) | $\delta_p$ (fm) | $\delta_n$ (fm) | $M_n/M_p$ Present results | $M_n/M_p$ Gazzaly *et al*[a] | $M_n/M_p$ Bernstein *et al* |
|---|---|---|---|---|---|---|---|---|
| $^{58}$Ni | 1·45 | $2^+$ | 0·773 | 0·711 | 0·831 | $1·25 \pm 0·19$ | $1·29 \pm 0·06$ | $1·35 \pm 0·15$[b] |
| | 2·46 | $4^+$ | 0·312 | 0·276 | 0·346 | $1·34 \pm 0·20$ | $1·15 \pm 0·45$ | |
| $N/Z = 1·071$ | 3·26 | $2^+$ | 0·407 | 0·400 | 0·414 | $1·11 \pm 0·18$ | $0·92 \pm 0·18$ | |
| | 4·52 | $3^-$ | 0·656 | 0·685 | 0·629 | $0·98 \pm 0·14$ | $0·95 \pm 0·11$ | |
| $^{90}$Zr | 2·19 | $2^+$ | 0·449 | 0·495 | 0·412 | $1·04 \pm 0·26$ | $1·12 \pm 0·04$ | $0·95 \pm 0·08$[b] |
| $N/Z = 1·250$ | 2·75 | $3^-$ | 0·701 | 0·980 | 0·478 | $0·61 \pm 0·29$ | $1·06 \pm 0·06$ | |
| $^{116}$Sn | 1·20 | $2^+$ | 0·645 | 0·598 | 0·680 | $1·50 \pm 0·28$ | | $1·75 \pm 0·08$[b] |
| $N/Z = 1·320$ | 2·27 | $3^-$ | 0·776 | 0·667 | 0·858 | $1·70 \pm 0·24$ | | |
| $^{208}$Pb | 2·61 | $3^-$ | 0·722 | 0·807 | 0·667 | $1·27 \pm 0·18$ | $1·72 \pm 0·07$ | |
| $N/Z = 1·537$ | 4·09 | $2^+$ | 0·532 | 0·411 | 0·611 | $2·28 \pm 0·43$ | $1·97 \pm 0·16$ | $1·50 \pm 0·30$[c] |

[a] Gazzaly *et al* (1982); [b] Bernstein *et al* (1981); [c] Madsen *et al* (1983).

results are in general consistent with the findings of Bernstein *et al* (1981b) that the $\delta$'s are probe-dependent.

## 4. Conclusion

We have reported here the elastic and the inelastic scattering angular distribution data for 270 MeV $^3$He particles from $^{58}$Ni, $^{90}$Zr, $^{116}$Sn and $^{208}$Pb targets. The optical model analysis of the elastic scattering data has been carried out and the systematics of the volume integrals of the $^3$He-nucleus optical potentials in the energy region of 100 and 270 MeV has been established. Macroscopic collective model analysis of the inelastic scattering data using the optical model parameters determined from the analysis of the elastic scattering data has led to reasonable reproduction of the data. The $B$(EL) values determined for the various low-lying levels are in good agreement with the other determinations obtained using different projectiles at various bombarding energies. This confirms the validity of the use of macroscopic collective model for the analysis of inelastic excitation by 270 MeV, $^3$He projectile.

## Acknowledgment

This work was supported by the National Science Foundation, USA and the Department of Atomic Energy, India.

## References

Afanasev V D, Afanasev N G, Gulkarov I S, Savitskii G A, Khvastunov V M, Shevchenko N G and Khomich A A 1970 *Sov. J. Nucl. Phys.* **10** 18

Bent R D, Pile P H, Pollock R E and Debevec P T 1981 *Nucl. Instrum. Methods* **180** 397
Bernstein A M 1969 *Advances in nuclear physics* (eds) M Baranger and E Vogt (New York: Plenum Press) Vol. II
Bernstein A M, Brown V R and Madsen V A 1981a *Phys. Lett.* **B103** 255
Bernstein A M, Brown V R and Madsen V A 1981b *Phys. Lett.* **B106** 259
Bhattacharya S and Kailas S 1983 *Z. Phys.* **A309** 325
Bingham C R, Halbert M L and Quiton A R 1969 *Phys. Rev.* **180** 1197
Crannell H, Helm R, Kendall H, Oeser J and Yearian M 1961 *Phys. Rev.* **123** 923
Curtis T H, Eisenstein R A, Madsen D W and Bockelman C K 1968 *Phys. Rev.* **184** 1162
Djaloeis A, Didelez J P, Galonsky A and Oelert W 1978 *Nucl. Phys.* **A306** 221
Fujita Y, Fujiwara M, Morinobu S, Katayama I, Yamazaki T, Itahashi T, Ikegami H and Hayakawa S I 1985 *Phys. Rev.* **C32** 425
Gazzaly M M, Hintz N M, Kyle G S, Owen R K, Hoffmann G W, Barlett M and Blanpied G 1982 *Phys. Rev.* **C25** 408
Gupta S K and Murthy K H N 1982 *Z. Phys.* **A307** 184
Gupta S K, Kailas S, Lingappa N and Shridhar A 1985 *Phys. Rev.* **C31** 1965
Harakeh M N, Van Heyst B, Van der Borg K and Van der Woude A 1979 *Nucl. Phys.* **A327** 373
Hodgson P E 1966 *Adv. Phys.* **15** 329
Hyakutake M, Matoba M, Kumabe I, Fukada M, Komatuzaki T, Yamagata T, Tanaka M, Inoue M, Miura I and Ogata H 1978 *Nucl. Phys.* **A311** 161
Hyakutake M, Kumabe I, Fukada M, Komatuzaki T, Yamagata T, Inoue M and Ogata H 1980 *Nucl. Phys.* **A333** 1
Jarvis O N, Harvey B G, Hendrie D L and Mahoney J 1967 *Nucl. Phys.* **A102** 625
Kunz P D 1982 DWUCK-4 Univ. of Colorado
Langevin-Joliot H, Gerlic E, Guillot J, Sakai M, Van de Wiele J, Devaux A, Force P and Landaud G 1982 *Phys. Lett.* **B114** 103
Liljestrand R P, Blanpied G S, Coker W R, Harvey C, Hoffmann G W, Ray L, Glashausser C, Adams G S, Bauer T S, Igo G, Pauletta G, Whitten C A, Oothoudt M A, Wood B E and Nann H 1979 *Phys. Rev. Lett.* **42** 363
Madsen V A, Suzuki T, Bernstein A M and Brown V R 1983 *Phys. Lett.* **B123** 13
Schwandt P 1981 Indiana University Cyclotron Facility Report No. 81-3
Sinha B, Srivastava D K and Ganguly N K 1973 *Phys. Lett.* **B43** 113
Wiencke H, Blok H P and Blok J 1983 *Nucl. Phys.* **A405** 237
Willis N, Brissaud I, Bornec Y Le, Tatischeff B and Duhamel G 1973 *Nucl. Phys.* **A204** 454